

# Modelling and experimental analysis of low concentrating solar panels for use in building integrated and applied photovoltaic (BIPV/BAPV) systems

Homan Hadavinia, Harjit Singh\*

College of Engineering, Design and Physical Sciences, Brunel University, London, UK

## ARTICLE INFO

### Article history:

Received 29 September 2018

Received in revised form

13 January 2019

Accepted 22 February 2019

Available online 27 February 2019

### Keywords:

Ray tracing

Compound parabolic concentrator

V-trough concentrator

Concentrating photovoltaics

BIPV

BAPV

## ABSTRACT

Geometrically equivalent V-trough and compound parabolic concentrators (CPC) were simulated to characterise the variation in optical efficiency using ray tracing modelling with COMSOL Multiphysics. The effect of CPC truncation and V-trough side wall angles were studied. The truncated CPC demonstrated much improved light acceptance outside the designed angle of acceptance when compared to the original CPC design and V-trough-like characteristics past the original design acceptance angles, consequently reducing material consumption for the manufacture of truncated CPC and therefore reduction in the cost of the system. Truncated CPCs showed optical efficiency equal to their full height counterparts, but a lower concentration ratio (4 at full, 3.6 at half and 2.7 at 50 mm height) due to an equivalent reduction of the inlet aperture size. The V-trough had a higher optical concentration ratio over 15–30° angle of incidents (AoI), with the CPC taking over from 30° AoI upwards. Experiments were performed on a 50 mm truncated CPC and a 22° Trough Wall Angle (TWA) V-trough collector under outdoor conditions. Experimentally measured data showed good correlation with ray tracing simulation results. Both experimental and the ray tracing analyses showed the CPC concentrator achieving a 2.4% higher power output compared to the V-trough design.

© 2019 Elsevier Ltd. All rights reserved.

## 1. Introduction

From the total renewable power generation capacity of 1081 GWp (not including hydro) in 2017 [1], solar photovoltaic (PV) accounted for approximately 402 GWp (37.2%) and concentrating solar thermal power technologies about 4.9 GWp. Concentrating Photovoltaic (CPV) technology has entered the market as a utility scale option for the generation of electricity with more than 370 MWp in cumulative installations, including several sites with larger than 30 MWp installed capacity [2]. The top highest electricity production capacity is at Golmud 1 plant (57.96 MWp) and Golmud 2 plant (79.83 MWp) in the Qinghai province (China) and Touwsrivier project (Western Cape, South Africa) at a capacity of 44.19 MWp. A key advantage of a CPV system is its higher conversion and optical efficiency. For a given peak power rating, a CPV system requires less land area than other photovoltaic technologies. Fresnel

and other lens-based imaging optical concentrators account for majority of the CPV installations worldwide. Most of the CPVs actively track the Sun in order to achieve meaningful concentration throughout the day. However, an active solar tracking mechanism adds to the capital and operating and maintenance costs while consuming a certain fraction of the generated power [3]. Therefore, nonimaging and stationary techniques of concentrating solar radiation are more effective, especially for installation on buildings. Application of the nonimaging optics can deliver moderate level of concentration (<10) with stationary concentrators requiring no maintenance of moving parts such as sun-tracking mechanisms, making them most suitable for buildings.

The key principle of CPV is the use of cost-effective concentrating optics that reduces the PV cell area, offsetting the high cost multi-junction solar cells made from heavily mined and relatively rare metals with relatively cheap optical systems, enabling the achievement of a levelized cost of electricity (LCOE) competitive with standard flat-plate PV technology [2,4]. The theoretical limit associated with solar-to-electricity conversion with an infinite number of junctions have a limiting efficiency of 86.8% under highly concentrated sunlight [5–7] while lab examples of multi-junction

\* Corresponding author.

E-mail addresses: [Homan.Hadavinia@brunel.ac.uk](mailto:Homan.Hadavinia@brunel.ac.uk) (H. Hadavinia), [Harjit.Singh@brunel.ac.uk](mailto:Harjit.Singh@brunel.ac.uk) (H. Singh).

cells have demonstrated performance over 46% under concentrated sunlight [8].

Many researchers have used ray-tracing technique for theoretical characterisation of a concentrating system for PV applications [9,10] while others used experimental optical efficiency and solar energy flux distribution by various methods [10–12]. Al-Shohani et al. [13] used OptisWorks ray tracing software to determine the optimum design of the V-trough concentrator. Sangani and Solanki [14] reported a 2-sun V-trough concentrator, which showed a 44% increased electrical output leading to a 24% overall reduction in cost of electricity. Mallick et al. [15,16] studied a 2-sun CPC leading to a 62% yield increase.

Building Integrated Photovoltaics (BIPV) are PV systems integrated into building elements such as roofs and building facades or the building materials themselves [17]. In contrast Building Applied Photovoltaics (BAPV) are applied over traditional elements of a building, usually applied post-construction rather than during the original building construction [18,19]. The cost of a BIPV system can be lowered by reducing PV module and component manufacturing costs, operation and maintenance costs and improving PV and other component efficiencies [20].

In this research, two geometrically equivalent non-imaging V-trough and CPC concentrators are investigated, using COMSOL Multiphysics computational tool and experimentally, with a target of increasing the efficiency of solar cells employed in BIPVs. Several concentrator geometries and configurations are studied at the relevant angles of incidence (AoI) of the incoming solar radiation. For CPC, three configurations are presented based on a 4-concentration ratio system. In addition, the effects of truncation of CPC reflector walls and V-trough Trough Wall Angle (TWA) are also investigated. The results of ray tracing analysis are used for designing and manufacturing of a CPC and a V-trough systems and outdoor experiments have been carried out on these systems to understand their optical and energy conversion characteristics. Finally, the results of ray tracing analysis are compared with the experimental results.

## 2. Geometries of V-trough and CPC concentrators

V-trough concentrators made from linearly inclined reflectors to concentrate light from a wider inlet aperture to a narrower absorber area (Fig. 1).

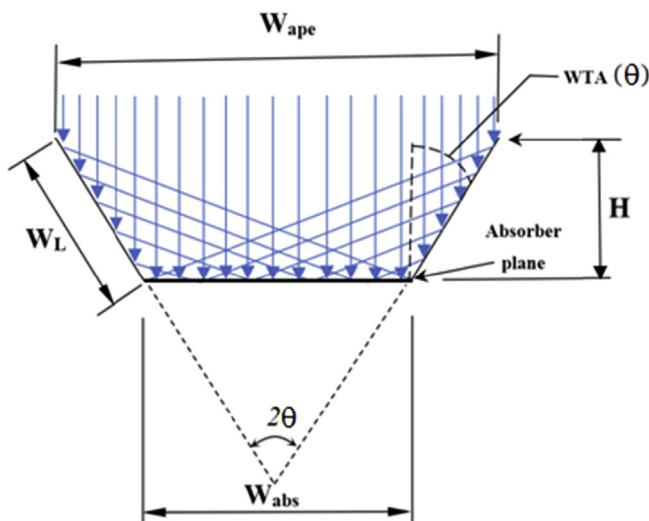


Fig. 1. Schematic of a V-trough concentrator cross-section.

The CPC is so called due to the inclusion of two parabolic reflectors in the system. It is designed such that the focal point of one parabola is the base of the opposing one. Fig. 2 shows the CPC comprised of two parabolas,  $PQ$  with focal point  $Q'$ , and  $P'Q'$  with focal point  $Q$ . These parabolas are rotated by the acceptance half angle  $\theta_h$ , with focal length  $f$  from the vertex of the parabola (A) to its focus (Q). CPC is considered the best static concentrator for solar radiation collection due to high optical efficiency and the capability to collect both diffuse and direct radiations [21,22]. Simultaneous work was done on CPCs by Hinterberger & Winston in 1966 [6,23] and Baranov [24] and Baranov and Melnikov [25] in 1965 and 1966, respectively. This led to a publication on the suggestion of 3D CPC (termed as *Parabolotoroidal mirrors*) in 1966 by Baranov [26]. Finally, in 1974 the 2D CPC geometry was described by Winston [27]. A comprehensive and up-to-date review of CPC design principles for miscellaneous configurations, applications, performance

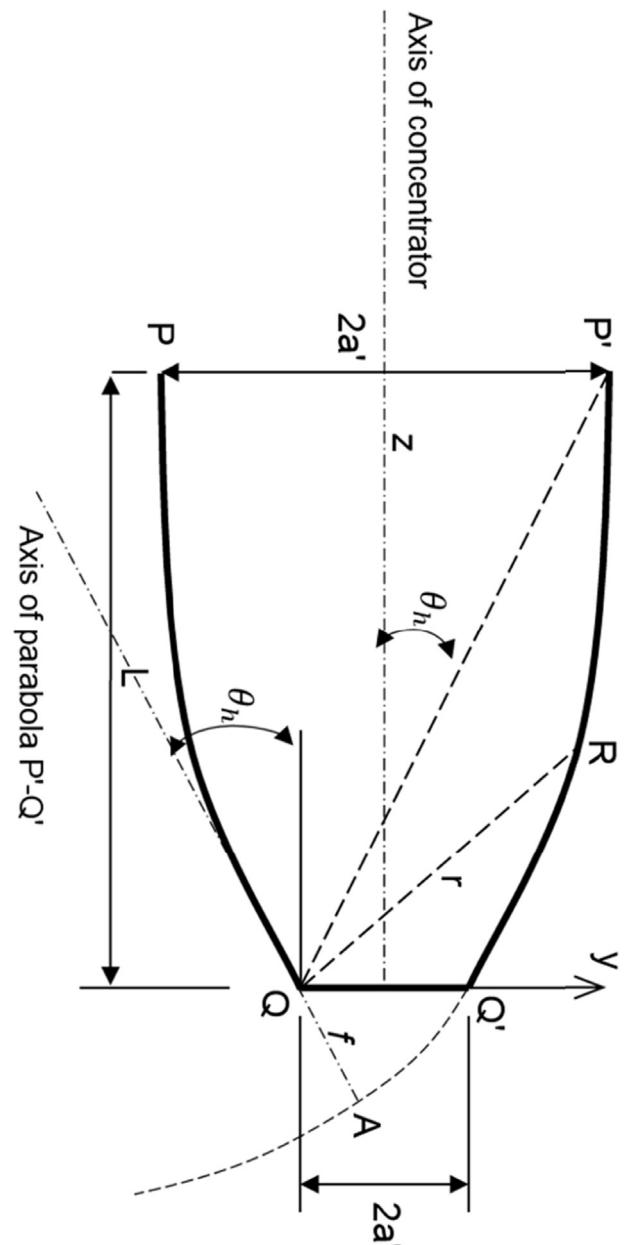


Fig. 2. Schematic of a CPC cross-section.

predictions and technological advances are presented in Ref. [28].

### 3. Ray trace modelling

In ray trace modelling hundreds or thousands of different rays are simulated and optical physics are used to predict how each ray interacts at each surface in the model domain. In this research, ray trace modelling is used to investigate the performance of full height and truncated CPC and V-trough concentrators. From these analyses, the power output of each design is calculated, the distribution of light on the solar cell is considered and the results are verified with the experimental measurements.

#### 3.1. Parametric driven geometry

The number of simulations required to model every design over the wide array of conditions is prohibitively large. For the V-trough, modelling Aol of 0–45° and TWA of 0–45°, a total of 46 × 46 (=2116) simulations are required. This is assuming only symmetrical V-trough is to be considered. If asymmetrical V-troughs (those with left and right reflector sides having different lengths) are modelled then the total simulations required would grow exponentially. The same principle applies to CPC concentrators; every CPC design and every truncation level needs to be modelled for every Aol.

A novel approach was used to convert the geometries in both 2D and 3D from manual CAD drawings to parametrically driven geometries. The aim once completed is that the solver (COMSOL Multiphysics) is given a range of various parameters and is able to automatically create and update the geometries and boundary conditions, allowing significant numbers of simulations to run automated.

##### 3.1.1. V-trough concentrator

For the purpose of modelling, four parameters, *inlet light*, TWA ( $\theta$ ), *wall length* ( $W_L$ -Fig. 1) and *wall length horizontal component* ( $W_x$ ), were defined as described in Eqs. (1) and (2) assuming the acceptable height for BIPV application is H = 50 mm.

$$W_L = \frac{50}{\cos(\theta)} \tag{1}$$

$$W_x = W_L \sin(\theta) \tag{2}$$

The V-trough was then implemented in COMSOL Multiphysics as a *Bezier polygon* consisting of the components shown in Fig. 3(a) and described as follows.

- A. (0,0) to (25,0) representing the 25 mm wide horizontally aligned solar PV cell receiver
- B. (25,0) to (25 +  $W_x$ ,50) representing the right-side wall of the V-trough
- C. (25 +  $W_x$ , 50) to (- $W_x$ , 50) going back twice the horizontal component of the reflectors as well as 25 mm receiver
- D. (- $W_x$ , 50) to (0, 0) reaching the left-most side of the solar receiver

##### 3.1.2. CPC concentrator

The geometry of the CPC, Fig. 3(b), requires the rotation of the parabolas by the acceptance half angle, as such the equation of the parabola is changed. Absolute values for the 50 mm CPC design selected are provided in parenthesis, derived from the equations below.

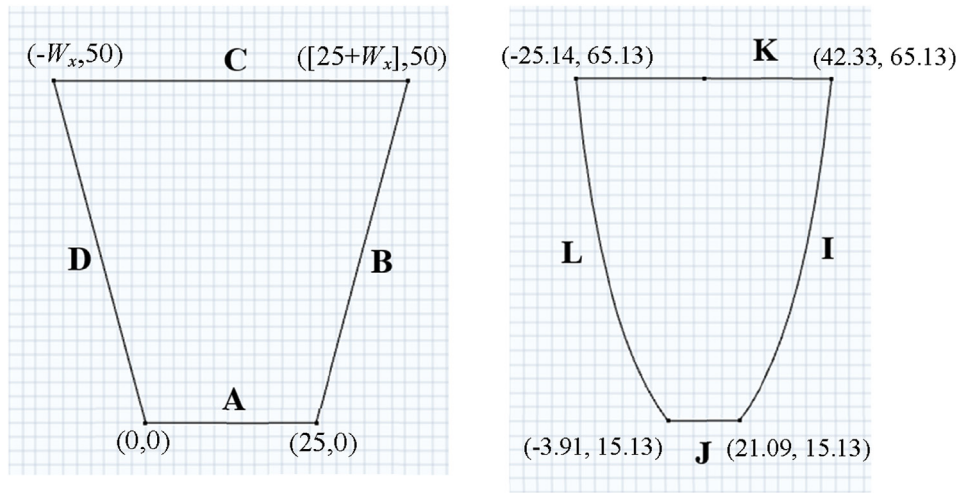
A rotation matrix derived from the Euler Formula in two dimensions takes the form:

$$R_\theta = \begin{bmatrix} \cos \theta & -\sin \theta \\ \sin \theta & \cos \theta \end{bmatrix} \tag{3}$$

This is used to get the new  $x$  and  $y$  coordinates (denoted as  $x'$  and  $y'$ ) by multiplication with the column vector:

$$v' = R_\theta v_0 \tag{4}$$

Furthermore, once a function is rotated, the result need not be a function i.e. a function has one  $y$ -point for every  $x$ -point, once rotated, it is possible an  $x$  value has more than one  $y$  value. As such, the parabola will take a parametric form; rather than  $x \rightarrow y(x)$ , the parabola will be described in the form  $s \rightarrow (x(s), y(s))$ .



(a) V-trough parameter schema

(b) CPC parameter schema

Fig. 3. Annotated (a) V-trough and (b) CPC schematics in COMSOL Multiphysics Geometry.

The parametric form of the rotated parabola is derived by:

$$\begin{bmatrix} x' \\ y' \end{bmatrix} = \begin{bmatrix} \cos \theta & -\sin \theta \\ \sin \theta & \cos \theta \end{bmatrix} \begin{bmatrix} x \\ y \end{bmatrix} \quad (5)$$

This leads to

$$a \left( -f \sin(\theta_h) + \frac{W_{abs}}{2}, \sin(-\theta_h) \cdot (-top_{root}) + \cos(-\theta_h) \cdot \frac{(-top_{root})^2}{4f} \right)$$

to

$$\left( \cos(\theta_h) top_{root} - \sin(\theta_h) \frac{top_{root}^2}{4f}, \sin(\theta_h) top_{root} + \cos(\theta_h) \frac{top_{root}^2}{4f} \right)$$

$$b \left( -f \sin \theta_h, f \cos(\theta_h) \right) \text{ to } \left( -f \sin(\theta_h) + W_{abs}, f \cos(\theta_h) \right)$$

$$c \left( -f \sin(\theta_h) + W_{abs}, f \cos(\theta_h) \right) \text{ to } \left( -2f \sin(\theta_h) + W_{abs}, 0 \right)$$

K. Inlet half-aperture set up as a 1-step Bezier Polygon:

$$x' = x \cdot \cos(\theta) - y \cdot \sin(\theta)$$

$$y' = x \cdot \sin(\theta) + y \cdot \cos(\theta) \quad (6)$$

Automating the truncation of the CPCs was achieved by creating a parametric curve within COMSOL Multiphysics with a minimum and maximum plot value. The maximum value represented the height of the truncated CPC for that simulation instance and the minimum the base (solar cell absorber width) of the CPC.

The maximum value was calculated by finding the *root* of the  $y'$  expression and substituting  $y_{top}$  for  $y'$ :

$$y_{top} = s \cdot \sin \theta + \frac{s^2}{4f} \cdot \cos \theta \quad (7)$$

The above quadratic equation was solved using the quadratic equation:

$$\frac{s^2}{4f} \cos \theta + s \cdot \sin \theta - y_{top} = 0 \quad (8)$$

$$s = \frac{-\sin \theta \pm \sqrt{\sin^2 \theta + \frac{y_{top} \cos \theta}{f}}}{\cos \theta / 2f} \quad (9)$$

The lower bound of the parametric curve was determined by the focal length of the CPC. This was the  $y$ -value of the rotated parabola which formed the base of the CPC. The process was applied again to find the cut-off point of the lower parabolas.

The symmetric CPC was then defined as a set of geometries as follows in sections I-L below:

I. First parabola set up as a *Parametric curve* drawn to  $top_{root}$ :

$$a \quad x = \cos(\theta_h)s - \sin(\theta_h) \frac{s^2}{4f}$$

$$b \quad y = \sin(\theta_h)s - \cos(\theta_h) \frac{s^2}{4f}$$

Where  $f$  is the focal length of CPC parabolas and  $\theta_h$  the CPC half acceptance angle.

J. Focal lines and absorber aperture set up as a *Bezier polygon* with segments:

$$a \quad (0, 0) \text{ to } (-f \sin \theta_h, f \cos \theta_h)$$

Where  $W_{abs}$  is the absorber width (PV cell width), set as 25 mm for the study.

L. For the symmetric CPC, the mirror transformation feature was used to get the opposing parabola and inlet aperture. In the case of non-symmetric CPC, a second parametric curve going to  $top_{root}$  was defined as:

$$a \quad x = \cos(-\theta_h)s - \sin(-\theta_h) \frac{s^2}{4f}$$

$$b \quad y = \sin(-\theta_h)s + \cos(-\theta_h) \frac{s^2}{4f}$$

Once set up, COMSOL Multiphysics can change the geometry and boundary conditions through a set of four core parameters: Aol  $angle_{light}$ , CPC concentration ratio  $C_r$ , PV cell width  $W_{abs}$  and truncation level (%). A 'parametric sweep' was used to run groups of simulations with COMSOL Multiphysics given ranges of each parameter to sweep.

### 3.2. Compound parabolic concentrator (CPC)

A symmetric CPC with concentration ratio of 4 ( $C_r=4$ ) and 25 mm wide absorber surface was considered. The geometric features of the concentrator are as follows:

- Half Acceptance angle:  $\theta_h = \sin^{-1}\left(\frac{1}{4}\right) = 14.478^\circ$
- Height of CPC:  $\frac{W_{abs} + W_{ap}}{2} \cot(\theta_h) = 242.06 \text{ mm}$

The CPC was modified by truncating the height profile at three levels; see Table 1, in order to achieve a BIPV/BAPV capable geometry.

All designs underwent ray tracing simulation in COMSOL Multiphysics using Geometric Optics for a maximum of 3 ns of ray propagation time. The concentrators were simulated under Aol ranging from  $0^\circ$  to  $45^\circ$ , see example results shown in Fig. 4. As the

**Table 1**  
CPC design parameters.

| CPC   | Cr  | Height (mm) | Height (%) | Cr (%) |
|-------|-----|-------------|------------|--------|
| Full  | 4   | 242.06      | 100%       | 100%   |
| Half  | 3.6 | 121.03      | 50%        | 90%    |
| 50 mm | 2.7 | 50          | 20.7%      | 67.5%  |

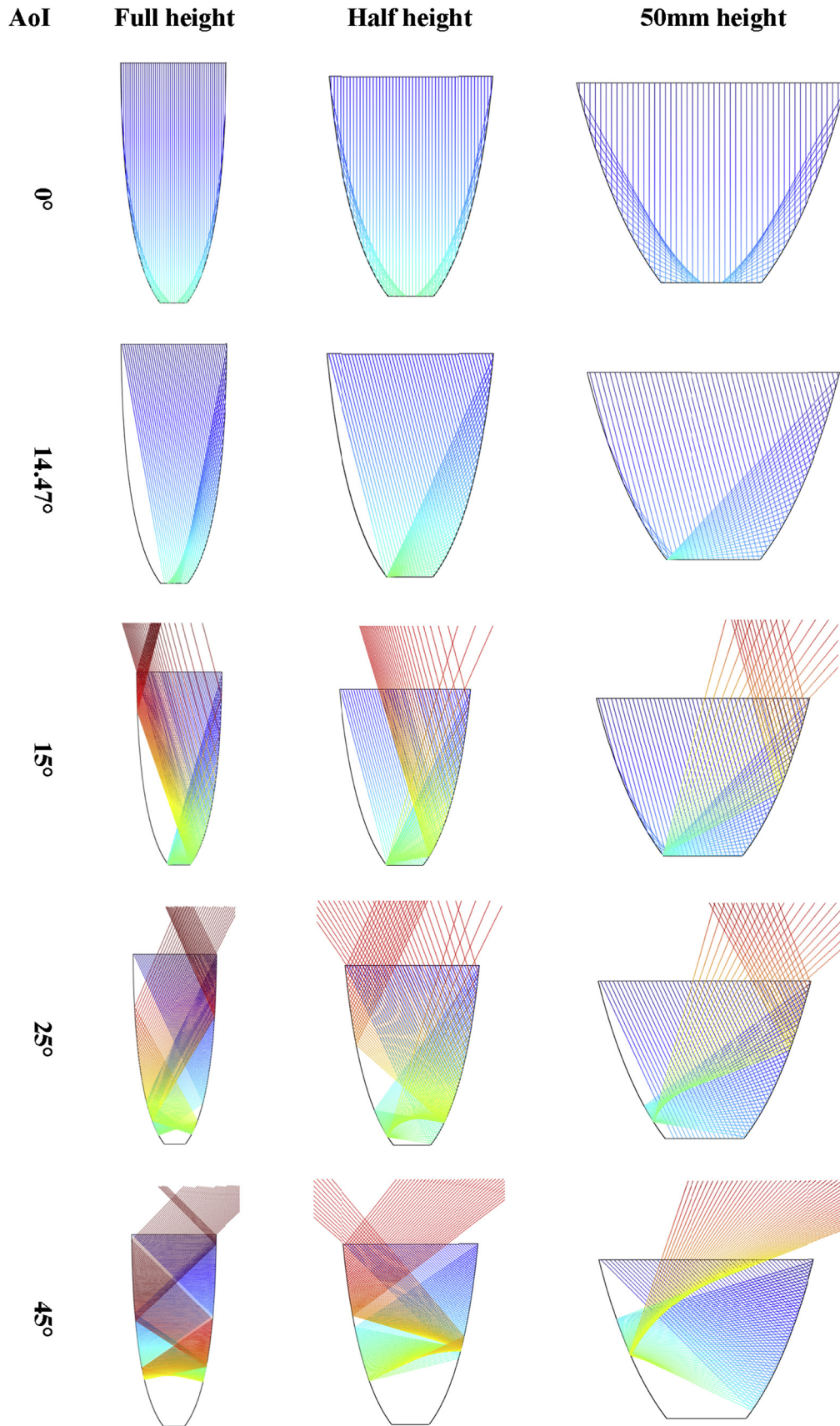


Fig. 4. Ray trace graphs of Full, Half and 50 mm height CPCs at a range of AoI.

CPC concentrators considered were symmetrical, this applies to either direction giving a 90° range for Aol, 45° from either direction.

In order to evaluate the accuracy of the model and compare with theoretical data, the Aol is divided into 10 discrete divisions, in step of 0.1° angular expanse, from 14° to 15°. Subsequently, the Aol was further divided into a hundredth of one degree between 14.47° and 14.48° to pin point the exact angle at which the design acceptance half angle is surpassed. In total, 64 different Aol were considered for each CPC design.

As expected, up to the CPC design half acceptance angle of 14.47° all rays were accepted – that is, the rays hit the absorber plane housing the solar cells. Within this 29° range (±14.5°), a 50% truncation of the reflector height resulted in only a 10% loss of concentration ratio and a reduction in the CPC height by 80% only reduced the concentration ratio by 1/3rd.

Beyond the half acceptance angle, the full height CPC showed a cliff-drop to zero output with all rays being reflected back out of the concentrator cavity. However, the truncated designs continued to partially accept sunlight with decreasing optical efficiency as the Aol increased. For example, the 50 mm height CPC continued to accept light up to Aol = 42°.

Another important measure of performance is the distribution of radiation intensity across the absorber plane; uneven distribution causes shading effects on the solar cells reducing their performance.

### 3.3. V-trough concentrators

The concentration ratio of the V-trough concentrator was varied

by changing TWA from 0° to 45°. Furthermore, each design was simulated at Aol over the range of 0°–45° making a total of 2116 computing simulations. The results of the simulation are presented in Fig. 5.

Fig. 6 demonstrates why some V-trough geometries start at lower optical efficiency in Fig. 5, such as the one with TWA of 45° starts at ~20%. At a TWA of 10°, the incident rays, which hit the reflector and eventually reach the absorber plane, land on the absorber at the same side as their corresponding reflector.

Ray acceptance should not constitute the final evaluation of a V-trough design. In fact, the geometric concentration ratio ( $C_r$ ) is not constant on all designs; as the TWA increases, so does  $C_r$ . If only the data shown in Fig. 5 are considered, then a wrong conclusion could be drawn that the best V-trough configuration is the one with TWA = 0°. However, the geometric concentration ratio of a 0° TWA V-trough concentrator will remain unity even at 100% ray acceptance, i.e. it will be a non-concentrating geometry. On the other hand, the 25° TWA V-trough had a  $C_r$  of 2.87, which though achieved an optical efficiency of 80% at Aol = 0° but is still significantly better than the 0° TWA V-trough in terms of ray concentration achieved. Optical concentration ratio as used in this research is defined as:

$$C_{opt} = \frac{\text{flux at receiver}}{\text{flux at aperture}} = C_r \cdot \eta$$

where  $\eta$  is the acceptance rate and  $C_r$  is the geometric concentration ratio.

Fig. 7 and Fig. 8 respectively present the geometric

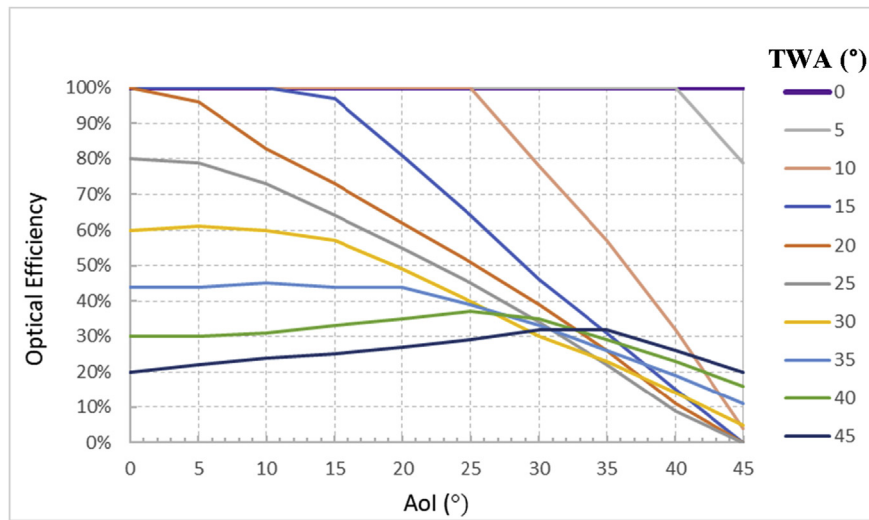


Fig. 5. The optical performance of V-trough configurations for various TWA and 0 < Aol < 45°.

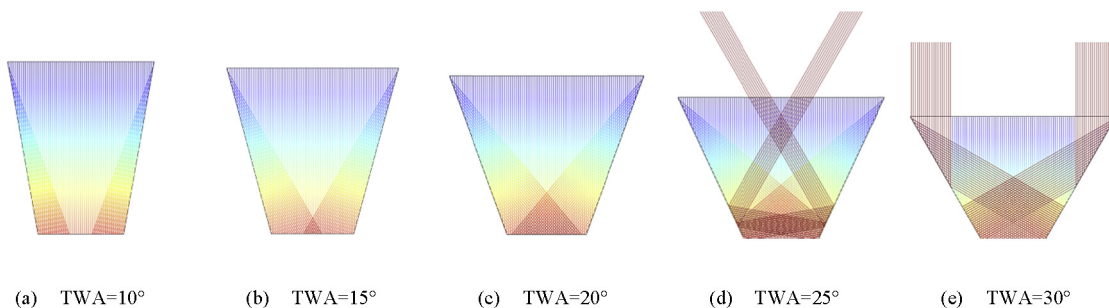


Fig. 6. Effect of varying TWA on the optical performance of V-trough concentrators at Aol = 0°.

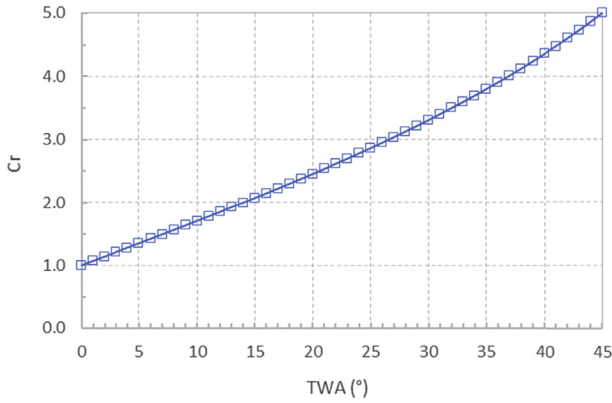


Fig. 7. Geometric concentration ratio of the V-trough geometries over the full range of  $0 < TWA < 45$ .

concentration ratios and the optical efficiencies of V-trough concentrators for the full range of TWAs studied.

The best performance was found to depend on the peak solar irradiance period for the location at which the concentrator is to be installed. As this varies, so too does the AoI of interest to the employer of the system.

With the earth rotating  $\sim 15^\circ/\text{hour}$  and assuming a 4-h peak solar irradiance, the corresponding AoI would vary over  $60^\circ$  equally distributed over the both sides of the peak solar irradiance time. To demonstrate the optical performance over this duration, results shown in Fig. 8 were filtered for AoI varying from  $0^\circ$  to  $30^\circ$  and the resulting optical concentration ratio obtained is shown in Fig. 9. Peak  $C_{opt}$  is the best concentration ratio normally at  $0^\circ$  AoI and Average  $C_{opt}$  referring to the averaged  $C_{opt}$  of the design over  $0-30^\circ$ .

This was followed by a deeper analysis with more rays and smaller TWA step of  $1^\circ$  over a range of  $15^\circ-25^\circ$ , whilst AoI was varied from  $0^\circ$  to  $30^\circ$  at  $20\times$  resolution ( $0.1^\circ$  AoI steps). The summary of the results is shown in Fig. 10.

It can be seen in Fig. 10(b), the best design is the one with TWA of  $22^\circ$  when considering average 4-h performance  $0-30^\circ$  AoI either direction for a V-trough with these geometric features:

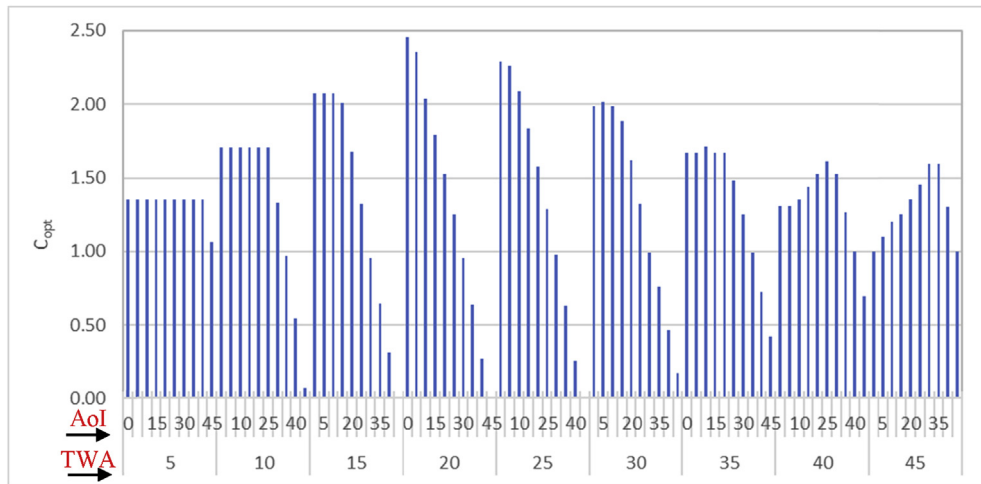
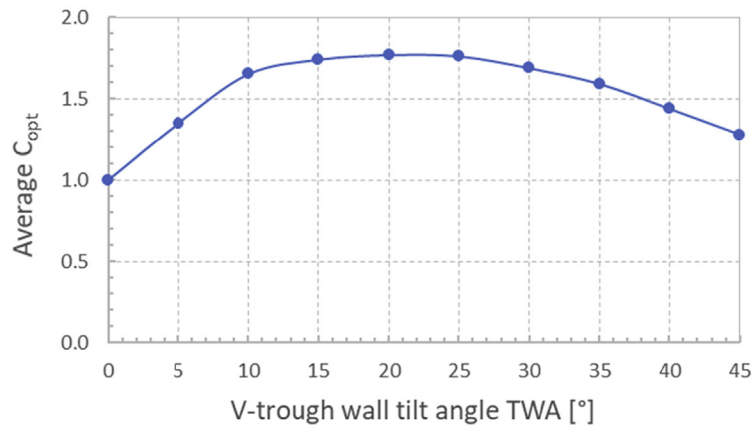


Fig. 8. Optical concentration ratio ( $C_{opt}$ ) of the V-trough concentrators for various TWAs (Major x axis) at different AoI (Minor x axis); angles are in  $^\circ$ .

| V-trough TWA | Average $C_{opt}$ |
|--------------|-------------------|
| 0            | 1.00              |
| 5            | 1.35              |
| 10           | 1.65              |
| 15           | 1.74              |
| 20           | 1.77              |
| 25           | 1.76              |
| 30           | 1.69              |
| 35           | 1.59              |
| 40           | 1.44              |
| 45           | 1.28              |

(a)



(b)

Fig. 9. Optical concentration ratio ( $C_{opt}$ ) of V-trough concentrators at AoI range of  $0^\circ$  to  $30^\circ$  (a) numerically and (b) graphically.

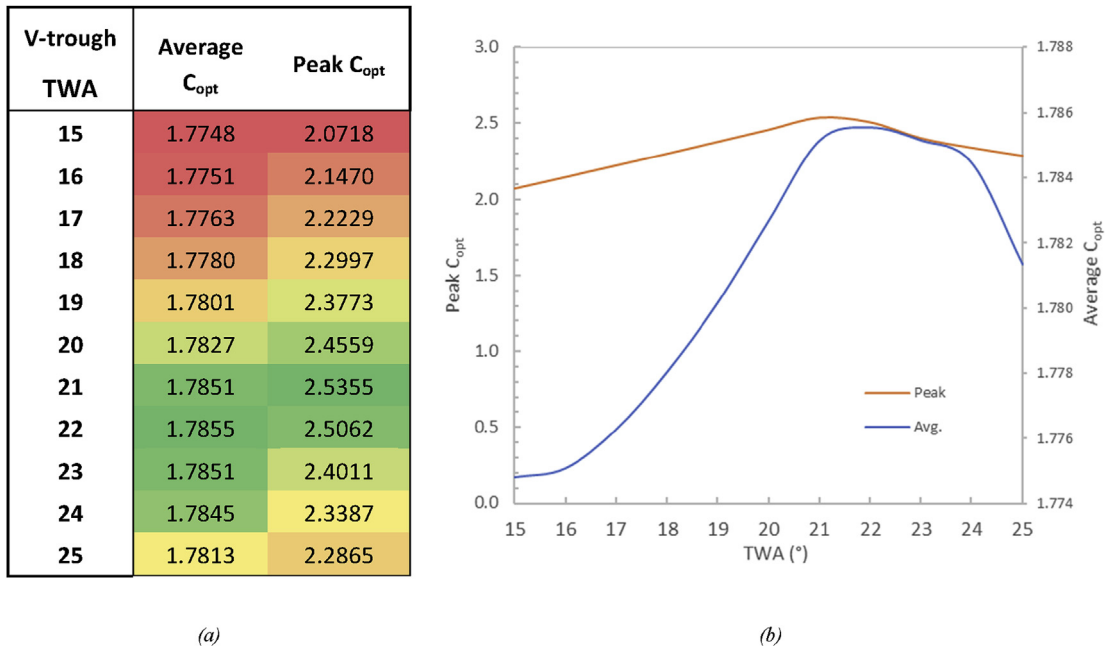


**Fig. 10.** High-resolution results for V-trough geometries (TWA 15–25°) for Aol varying from 0° to 30° in (a) tabular and (b) graphical format. Peak  $C_{opt}$  refers to the V-trough's best performance typically at 0° Aol, with Average  $C_{opt}$  referring to its average  $C_{opt}$  over 0–30° Aol.

- Height: 50 mm
- Absorber width: 25 mm; Aperture width: 65.4 mm
- Geometric Concentration Ratio  $C_r$ : 2.616
- Optical Concentration Ratio  $C_{opt}$ : Average: 1.786; Peak: 2.506

### 3.4. Comparison of V-trough and CPC concentrators

COMSOL Multiphysics ray tracing results for the performances of the CPCs and V-trough concentrators, in terms of  $C_{opt}$ , as a function of the Aol are shown in Fig. 11. It can be seen all CPC variants had 100% acceptance to all incident rays till Aol equals the design half acceptance angle of 14.47°. The untruncated CPC showed a cliff-drop to zero acceptance beyond this angle. On the other hand, the 22° TWA V-trough concentrator underwent a steady linear decline reaching zero acceptance at Aol  $\approx$  43°.

Truncation expectedly caused a significant improvement in the optical performance of CPC collectors outside of their 14.47° angle

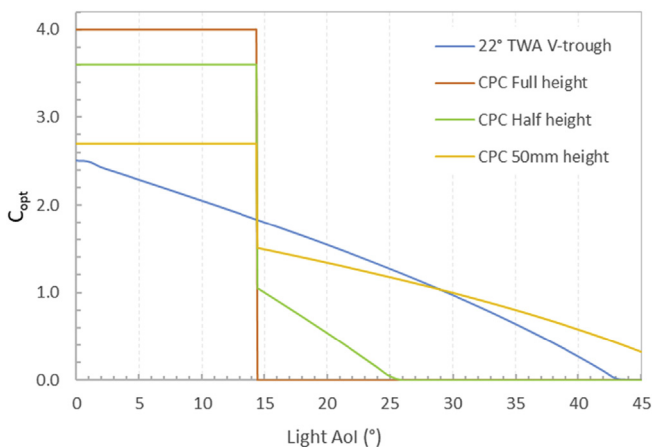


**Fig. 11.**  $C_{opt}$  of V-trough and CPC concentrators at various truncation levels.

of acceptance. All CPC showed a sudden drop in the performance for Aol greater than half acceptance angle, however, the truncated designs exhibited gradual decline in their performance of varying slopes rather than a cliff-drop in the acceptance. In fact, the half-truncated and 50 mm height CPC began to imitate V-trough-like behaviour. This, along with the lower height profile are the two primary arguments for adoption of such truncated CPCs for use in BIPVs.

In comparing the 50 mm CPC and 22° TWA V-trough it should be noted that the CPC has  $C_{opt} = 2.7$  vs. V-trough of 2.5 at Aol of 0°. The optical concentration ratio of CPC remains constant up to its acceptance half angle of 14.47° while that for the V-trough concentrator dropping gradually to 1.8. At light Aol = 14.47°, the CPC cliff-drops sharply to  $C_{opt} = 1.5$  (vs. 1.8 for V-trough). Beyond light Aol = 14.47°, the CPC and V-trough both show gradual drops in performance, with V-trough having a steeper decline. Due to this steeper decline, the CPC catches in performance with the V-trough at 29° Aol ( $C_{opt} \sim 1.04$ ). Beyond Aol > 29°, the CPC again overtakes the V-trough in performance. Overall, even when considering up to 30° Aol, for the peak 4-h period, the CPC has 9.4% performance improvement over the V-trough concentrator. If larger Aol are considered, the 50 mm CPC will further its gains; even at Aol = 45°, the CPC can be seen as still accepting light as shown in Fig. 11.

Fig. 12 and Fig. 13 show the local flux concentration distribution along the width of the absorber (PV cell surface) at Aol of 0° and 10° for the concentrators. At Aol of 0°, the V-trough (green line) had a perfectly even distribution along the absorber width and the CPC systems had peaks near the edges of the absorber and bigger peaks mirrored at 10 mm and 15 mm positions. The causes of these peaks are discussed later in Fig. 14 and Fig. 15. As the Aol increases, the peaks become asymmetrical and shift in the opposite direction of the incoming light. Fig. 13 shows these shifts. The V-trough was still more uniform in terms of flux distribution at the absorber surface but had two distinct regions of acceptance, high local flux concentration over 0–13 mm and lower over 13–25 mm widths. This pattern continued as Aol was increased.

The central peaks shown in Fig. 12 occurred due to the focal

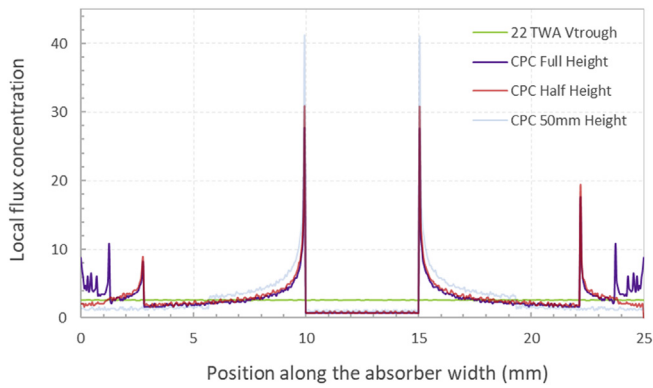


Fig. 12. Flux concentration distribution of 22° TWA V-trough and CPC at AoI = 0°.

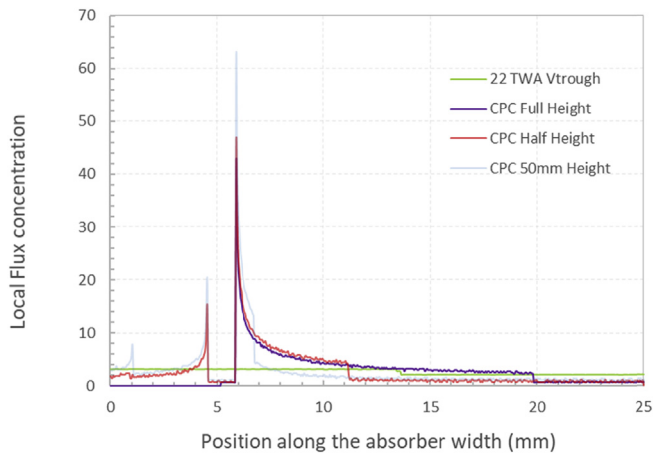


Fig. 13. Flux concentration distribution of V-trough and CPC at AoI = 10°.

region of the parabolic reflectors. This is the area the majority of the light rays hitting the reflectors surface (shown in Fig. 14). The

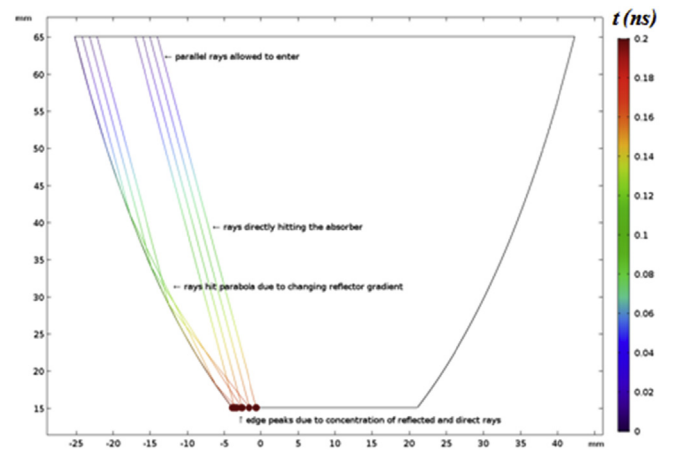


Fig. 15. Ray trace diagram subset demonstrating effect of parabolic curve and truncation on ray acceptance (example shown: 50 mm CPC at AoI = 10°).

location of the peaks changes for other values of AoI. The smaller peaks near the edges, shown in Fig. 12, are understood to be caused by overlapping rays entering the CPC at the top which are reflected due to the changing gradient of the parabola. These locations receiving the reflected and directly incident rays exhibited increased local flux concentration distribution. The causes of these peaks are presented in Figs. 14 and 15 with rays coloured based on time. As the AoI increases above 0°, the peaks become asymmetrical and shift in the opposite direction of the incoming light. Fig. 13 shows the shifts of the peaks to the left, due to light incidence on the CPC at AoI = 10° from the left towards the right (Fig. 15).

#### 4. Experimental studies

An experimental programme was undertaken to validate the results of computational models described above. CPC and V-trough concentrators were designed in CAD (SolidWorks) software with cross sections shown in Fig. 16. High-Density Polyurethane

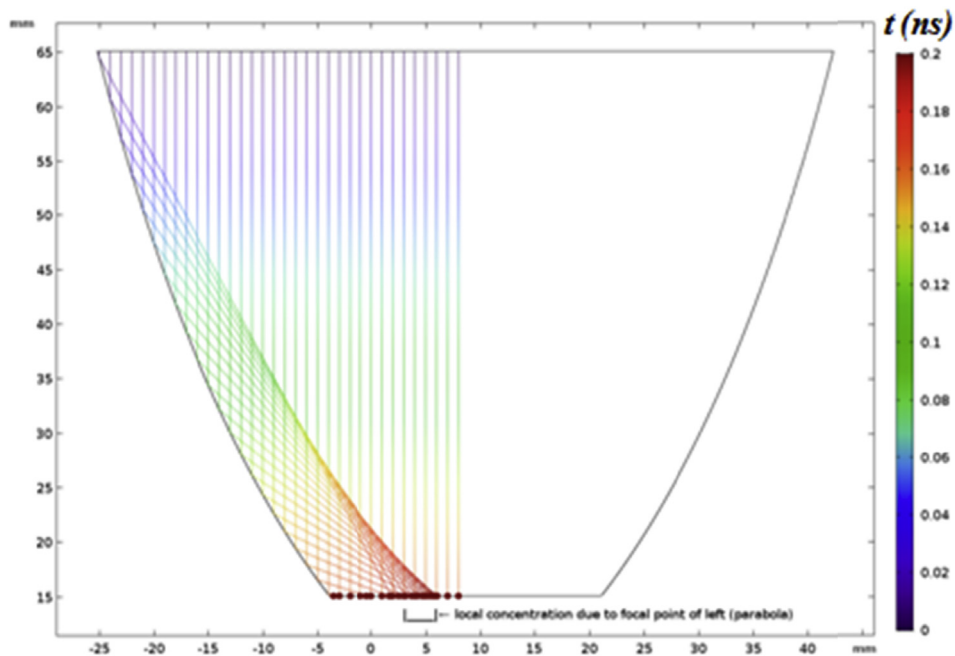


Fig. 14. Central flux concentration occurring due to focal regions of the reflector parabolas (example shown: 50 mm CPC at AoI = 0°).

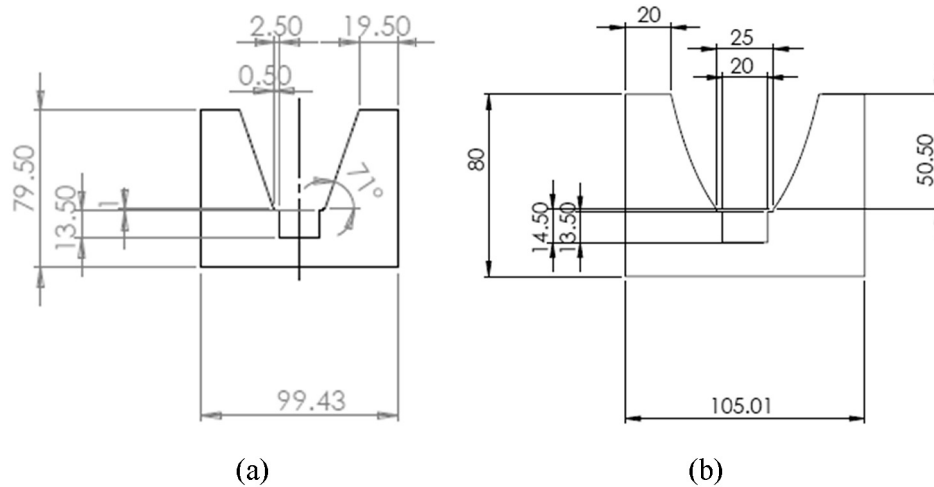


Fig. 16. Schematic drawings of (a) V-trough and (b) CPC (all dimensions in mm).

Model Board, commonly referred to as Uriel, was employed as the substrate material and profile substrates were manufactured using CNC milling machine. Uriel is thermally stable up to 130 °C, and further beyond with small losses in tensile strength. Particular attention was paid during cutting the CPC parabolas by adopting small step sizes during milling the troughs.

The PV cells obtained from BISOL [29] were cooled by passing water through a copper pipe welded to a copper plate housing the solar cells. The copper plate also helped in enhancing heat exchange between the PV cells and the coolant. Therefore, a 1 mm deep groove was provided in both the CPC and V-trough concentrators (Fig. 16) to accommodate the copper plate, the thermal paste and electrical insulation. The absorber area for both concentrators was 25 mm × 250 mm with solar cells purchased in standard 156 mm × 156 mm blocks. The PV cells were cut to 25 mm × 125 mm and two units connected in series to match with the absorber area. Since the Si-solar cells used are comprised of silicon wafers with aluminium back plating, the cutting was done using low power CO<sub>2</sub> laser machine to etch the front of the silicon and snap along the lines. To electrically insulate the solar cells from the copper plate while allowing the heat transfer, Mica electrical insulating film was sandwiched between the two. Mica sheets (MIC-20) purchased from RS Components & Controls Ltd rated at heat resistant up to temperature of 500 °C. Thermal paste was applied to both sides of the Mica sheet to ensure good physical contact for transfer of heat from solar cell to copper tube. The final assembled concentrator system is shown in Fig. 17.

Alanod Miro-Silver 2 4200AG with >98% total reflection [30] was used as the reflector surface in both concentrators. The Miro-Silver 2 sheet was glued to the concentrator substrate at respective reflector walls. The reflector sheets for CPC concentrator were pre-shaped using a bending machine prior to attachment to ensure they took the shape of the parabola prior to the adhesive's setting. The final concentrators are shown in Fig. 18.

The schematic presented in Fig. 19 shows the connectivity of all components in the experimental test unit developed during this research. The pyranometer attached measures total solar radiation, the second yellow cable running from the Pico data logger connects to the shaded pyranometer to measure diffuse solar radiation. A Keithley 2401 SMU acquisition system was employed to measure I-V characteristics of the solar cells.

Tables 2–4 provide the technical specifications of the two pyranometers and the Pico TC-08 data logger used.

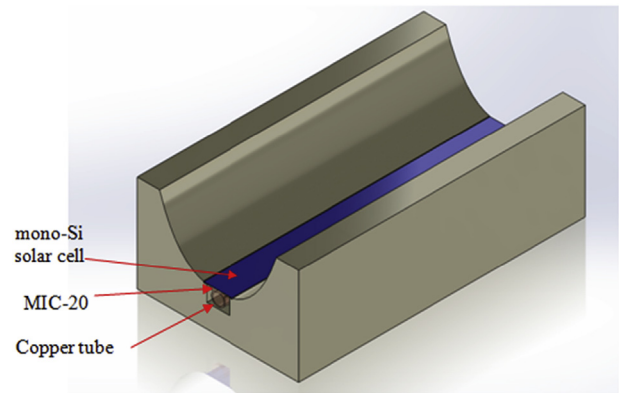


Fig. 17. Final Assembly of the concentrator system.

## 5. Comparison of experimental and modelling results

Ponce-Alcántara et al. [31] performed an experimental study of the effect of temperature variation with the performance of silicon solar cells. They presented the effect of temperature as a temperature coefficient of maximum power point ( $CTP_{mpp}$ ) with the power output defined as follows:

$$P_{mpp} = P_{mpp}(25^{\circ}\text{C}) \cdot [1 + CTP_{mpp}(T - 25^{\circ}\text{C})]$$

The temperature coefficient for c-Si was reported at  $\sim -0.45\%/^{\circ}\text{C}$ . Experimental studies were carried out considering the effects of cooling on LCPV performance. The readings were taken as close to solar noon (i.e. 0° angle of incidence) as possible. Table 5 presents the results of the CPC concentrator with the cooling pipe turned on and off. Solar noon on the 20th September 2017 occurred at 12:53 p.m. local time.

Results show the non-cooled CPC operates at  $-12.44\%$  power output (W) due to a temperature rise of 30.9 °C. This translates into a temperature coefficient of  $-0.40\%/^{\circ}\text{C}$ . Fig. 20 presents the I-V (and P-V) measurements for cooled and non-cooled CPC concentrator.

Fig. 21 shows the experimental direct and diffuse solar radiation data collected on the 20th Sept 2017, presented due to the clear skies on the day and good solar irradiance. Orange (diffuse) data was collected with a shaded pyranometer, blue (direct) data was total irradiance taken with pyranometer on plane of concentrator

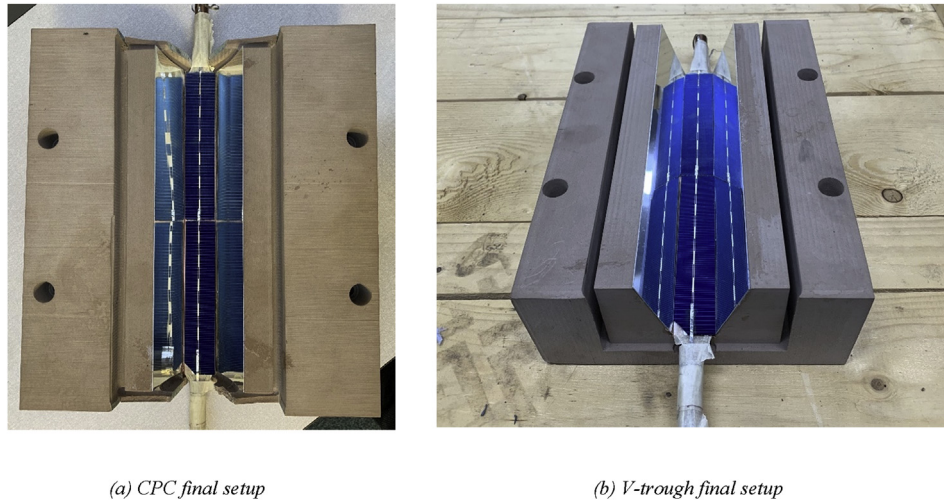


Fig. 18. Manufactured concentrators with solar cell, copper pipe, heat transfer copper plate and bus-bar junction: (a) CPC and (b) V-trough.

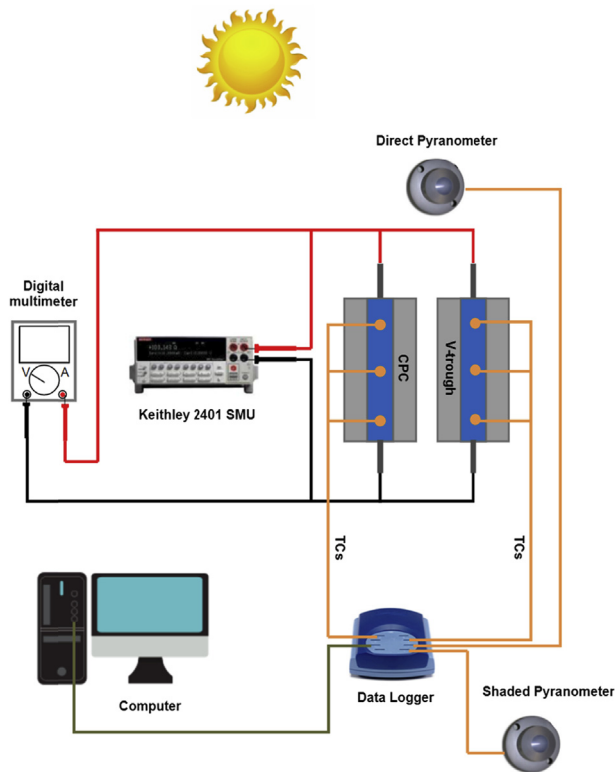


Fig. 19. Experimental setup employed to test the concentrators under realistic ambient conditions.

Table 2  
Pyranometer technical specifications.

| SP Lite2 Pyranometer  |  |
|---|--|
| Spectral range (overall)  | 400–1100 nm                              |
| Sensitivity   | 60–100 $\mu\text{V}/\text{W}/\text{m}^2$ |
| Response time SP Lite2 (95%)  | <500 ns                                  |
| Directional response (up to 80° with 1000 $\text{W}/\text{m}^2$ beam) | <10 $\text{W}/\text{m}^2$                |
| Temperature response  | < -0.15%                                 |
| Operational temperature range   | -40 °C to +80 °C                         |
| Maximum solar irradiance  | 2000 $\text{W}/\text{m}^2$               |
| Field of view   | 180°                                     |

Table 3  
Pico TC-08 data logger technical specifications.

|                         |  |
|-------------------------|--|
| Number of channels      | 8  |
| Conversion time         | 100 ms   |
| Temperature accuracy    | Sum of $\pm 0.2\%$ of reading and $\pm 0.5$ deg C        |
| Voltage Accuracy        | Sum of $\pm 0.2\%$ of reading and $\pm 10$ $\mu\text{V}$ |
| Resolution (Noise free) | 16.25 bits   |
| Operating temperature   | 0–50 deg C   |

Table 4  
TC-08 Pico data logger thermocouple resolution.

| Thermocouple type | Overall range °C | 0.1 °C resolution | 0.025 °C resolution |
|-------------------|------------------|-------------------|---------------------|
| B                 | 20 to 1820       | 150 to 1820       | 600 to 1820         |
| E                 | -270 to 910      | -270 to 910       | -260 to 910         |
| J                 | -210 to 1200     | -210 to 1200      | -210 to 1200        |
| K                 | -270 to 1370     | -270 to 1370      | -250 to 1370        |
| N                 | -270 to 1300     | -260 to 1300      | -230 to 1300        |
| R                 | -50 to 1760      | -50 to 1760       | 20 to 1760          |
| S                 | -50 to 1760      | -50 to 1760       | 20 to 1760          |
| T                 | -270 to 400      | -270 to 400       | -250 to 400         |

with diffuse radiation deducted.

Fig. 22 to Fig. 24 present the experimental power output of the CPC, flat-plate (non-concentrator) and V-trough modules. It can be seen that the power output of the flat plate solar cell is significantly lower. Conversely, the performance drop due to increased angle of incidence (solar time) is less and the power output of the flat plate solar cell tracks the solar irradiance throughout the day (see Fig. 23).

The measured power output of developed CPV concentrators, CPC and V-trough, and that calculated from ray-trace modelling are compared in Fig. 25. The ray tracing model output was converted to power by considering the system's real power conversion efficiency and optical efficiency based on:

$$\text{Power (W)} = \tau_g \times R_{spec} \times \eta \quad (10)$$

Where  $\tau_g$  is the glass transmittance, set to 100% for comparison to experiments,  $R_{spec}$  is the specular reflectance losses of the AlanoD reflector sheet (92%) and  $\eta$  is the solar cell power conversion efficiency set at 15% based on average measurements.

A good correlation between the experimental measurements and model power output results was found. The experimental CPC

**Table 5**  
CPC under cooled and non-cooled conditions 20th Sept 2017.

| TIME (LOCAL) | CONC   | TEMP(°C) | $I_{sc}$ | $V_{oc}$ | P (W) | DIRECT + DIFFUSE ( $W/m^2$ ) | DIFFUSE ( $W/m^2$ ) | DIFFUSE (%) |      |
|--------------|--------|----------|----------|----------|-------|------------------------------|---------------------|-------------|------|
| 12:45        | Cooled | CPC      | 32.32    | 1.61     | 1.2   | 1.932                        | 1102.61             | 104.31      | 9.5% |
| 12:45        | Heated | CPC      | 63.22    | 1.42     | 1.2   | 1.704                        | 1102.61             | 104.31      | 9.5% |

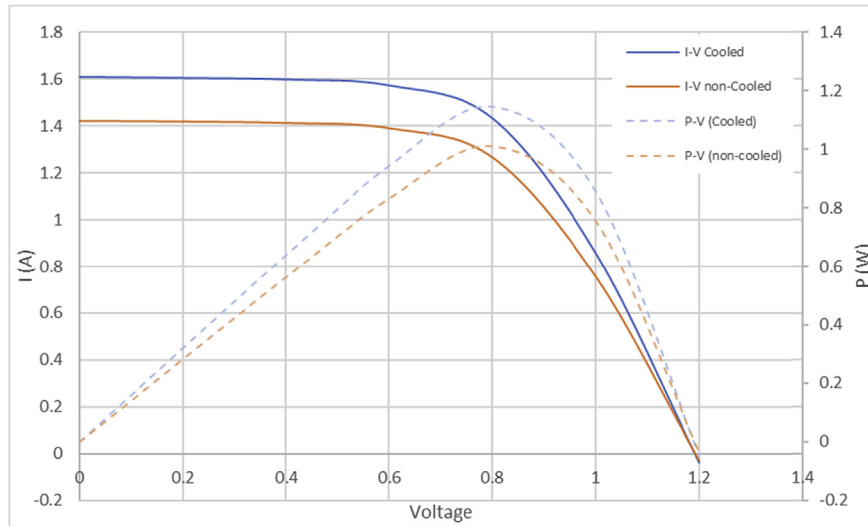


**Fig. 20.** I-V and P-V curves of 50 mm CPC with and without active cooling.

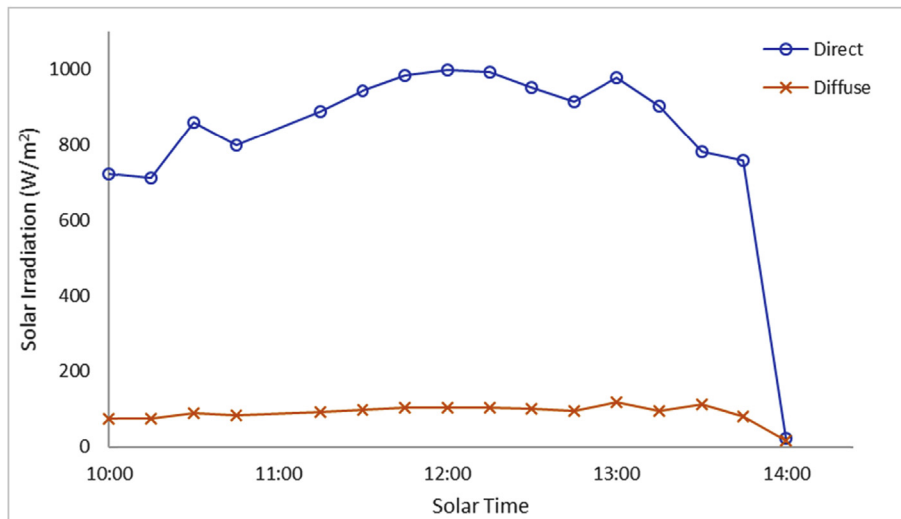


**Fig. 21.** Direct and diffuse solar radiation 20th Sept 2017.

measurements showed constant power output for  $AoI \sim \pm 15^\circ$ , in line with model results. The V-trough measurements showed a near linear drop with respect to light  $AoI$  changes in both directions. This was again in good corroboration with the model predictions.

On average the CPC showed a 2.4% higher power output than V-trough. However, this was lower than predicted by the COMLSOL Multiphysics ray tracing models. The most likely cause of the discrepancy is the increased energy flux non-uniformity of the CPC concentrators which resulted in reduction of power output of the

CPV system.

Similar studies were carried out by Singh et al. [32]. They showed that for the V-trough and CPC systems with the same geometrical concentration ratio, the V-trough concentrator had an electrical power output up to 17.2% higher than the CPC system at a specific tilt angle of  $30^\circ$  and the V-trough had a consistently higher receiver plate temperature. Redpath et al. [33] also showed that CPC integrated combi photovoltaic-thermal (PVT) had a lower thermal efficiency than flat plate PVT with a heat removal factor of 0.488 compared to 0.638 of the later.

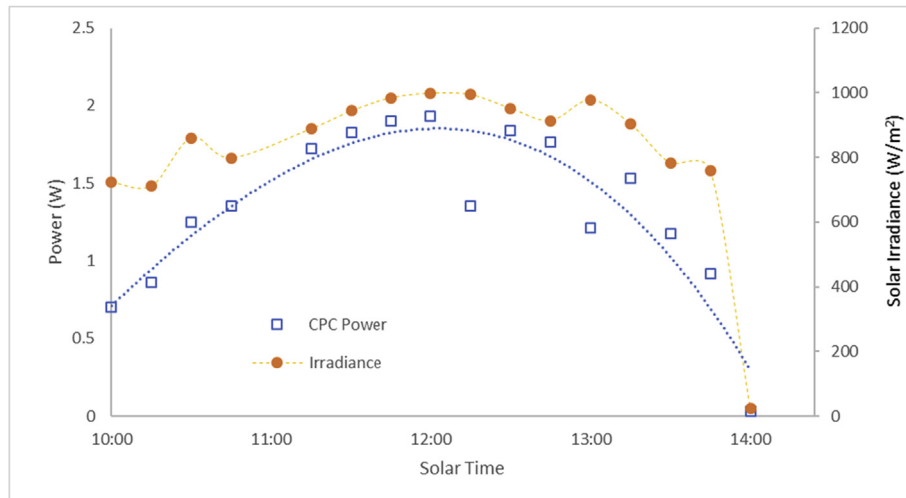


Fig. 22. Power output and solar irradiance for CPC for period 10:00 to 14:00 solar time.

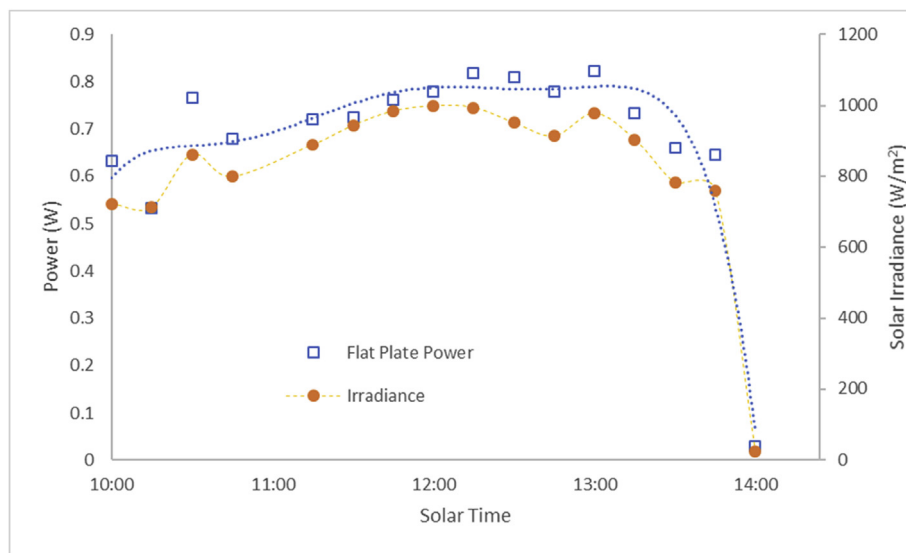


Fig. 23. Power output and solar irradiance for flat plate solar cell for period 10:00 to 14:00 solar time.

However, the results from the current research showed a better performance of CPC rather than V-trough. This could be down to geometric optimisations performed by COMSOL Multiphysics leading to a better prototype design. Another difference is that the CPC fabricated in this study was smaller in scale for BIPV integration, e.g. the absorber width was 25 mm compared to 125 mm used in Singh et al. [32].

## 6. Conclusion

The CPC and V-trough concentrators investigated in this study showed good robustness in their performance despite not tracking the sun. This makes them best candidates for BIPV/BAPV applications where such devices can be used as fixed concentrating generators since installing operating and maintaining tracking CPV systems is expensive and complex. Additionally, the low concentrating designs investigated can also harness a proportion of the incident diffuse radiation; a feature which is of particular interest for locations such as the UK and other northern maritime climatic zones.

A 50 mm truncated-CPC and 50 mm V-trough were contrasted and compared. It is shown that a drop in the performance of both concentrators occurs at increased angles of incidence (AoI). The drop beings at  $14.47^\circ$  for CPC and immediately for V-trough; however, the V-trough concentrator showed lower losses as incidence angle increased compared to non-truncated CPC systems.

The truncated CPC design proposed in this study furthers the advantages by improving acceptance from  $\pm 14.5^\circ$  to beyond  $\pm 45^\circ$ , although with diminishing returns. This comes at the cost of a reduction of concentration ratio, although the height profile reduction of 80% is a necessity for BIPV integration, for example, to fit CPV units within window gap or on vertical walls.

The results showed and quantified the increase in angle of acceptance, reductions in height profile and V-trough-like characteristics past the original CPC design acceptance angles, with consequence in reducing material consumption for the manufacture of CPC and therefore reduction in the cost of the system.

For ray tracing analysis a variety of direct and iterative solvers were tested, and the generalized minimal residual method was used for the analysis of concentrators. A drop of performance was

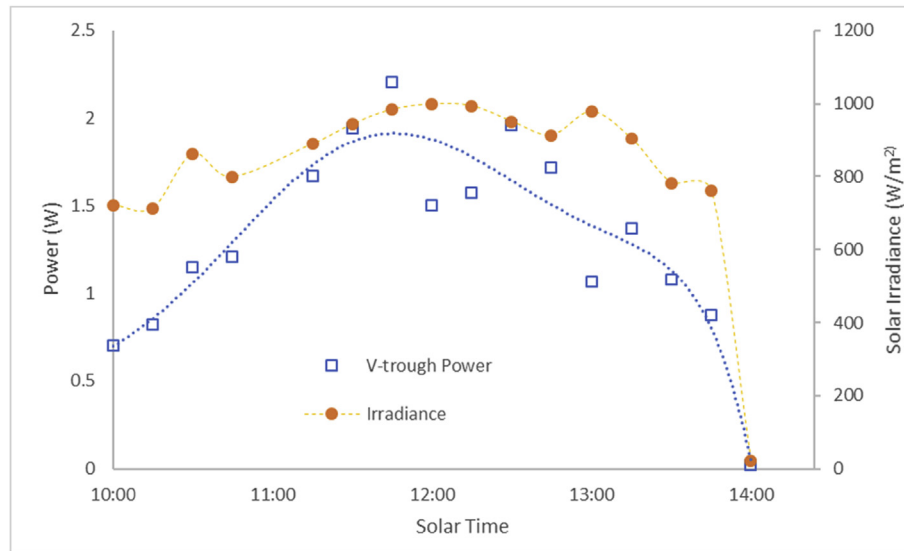


Fig. 24. Power output and solar irradiance for V-trough concentrator for period 10:00 to 14:00 solar time.

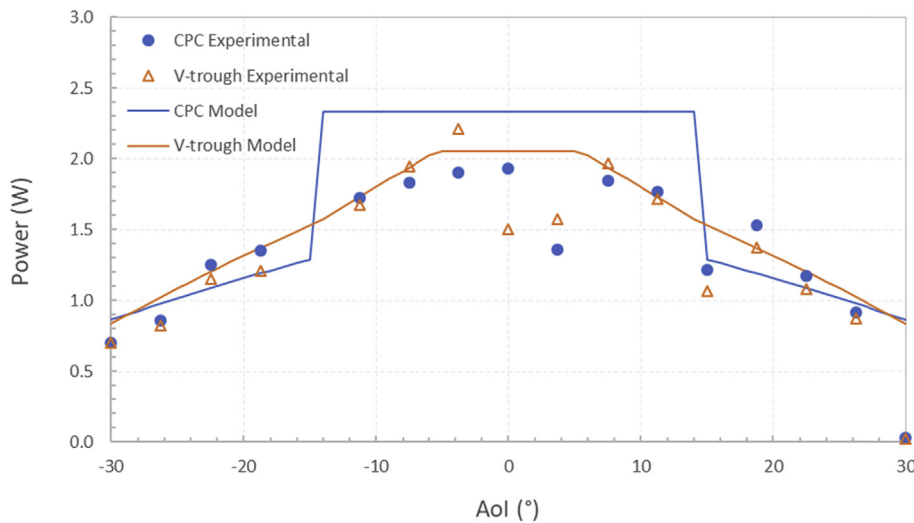


Fig. 25. Experimental and modelling power output from CPC and V-trough concentrators over various light angles of incidence.

observed for both concentrators at increased Aol; however, V-trough showed a better ability to dampen the loss as incidence angle increased. In terms of concentration ratio, a truncated CPC at equal height showed an optical concentration ratio of 2.70 whilst V-trough hovered around 2.38 resulting in a net performance increase of 13% for CPC adoption. Results showed V-trough having lower concentration ratios but better performance at high angles of incidence compared to CPCs. Truncated CPCs showed equal optical efficiency to their full height parents but a lower concentration ratio due to a reduction in inlet aperture size.

The modelled 50 mm CPC concentrator particularly designed for BIPV showed a greater overall concentrating performance, with significantly improved concentration for Aol up to the half acceptance angle, a small loss compared to the V-trough for Aol between half acceptance angle to 29°, and again an improvement over the V-trough from for Aol > 30°. All truncated CPCs also show V-trough-like behaviour past their acceptance angles, making them suitable for BIPV incorporation. On the other hand, the V-trough concentrator showed better uniformity of flux distribution, this was

especially pronounced at 0° Aol with flux distribution being perfectly uniform.

The experimental investigation was carried out on two concentrators, a CPC design and a V-trough one and for both systems the optical and energy conversion characteristics were experimentally measured. The analysis of the experimental power output data showed good correlation with ray tracing simulations, showing similar behaviour with changing Aol. CPC was found to have an overall 2.4% higher power output compared to V-trough concentrator. Although this was lower than the difference predicted by modelling analysis, the discrepancy was put down to the non-uniformity of the concentrated light on the CPC absorber plane and differences in contour and surface characteristics between the ideal and the manufactured parabolic reflectors.

#### Acknowledgement

First author thanks UK's Engineering and Physical Sciences Research Council's Doctoral Training Partnership programme to

fund his PhD study, which made this research possible.

## Appendix A. Supplementary data

Supplementary data to this article can be found online at <https://doi.org/10.1016/j.renene.2019.02.121>.

## References

- [1] REN21, Renewables 2018 Global Status Report, 2018. Available: [http://www.ren21.net/wp-content/uploads/2018/06/17-8652\\_GSR2018\\_FullReport\\_web\\_final\\_.pdf](http://www.ren21.net/wp-content/uploads/2018/06/17-8652_GSR2018_FullReport_web_final_.pdf). (Accessed 9 December 2018).
- [2] M. Wiesenfarth, S.P. Philipps, A.W. Bett, K. Horowitz, S. Kurtz, Current Status of Concentrator Photovoltaic (CPV) Technology, Fraunhofer Institute for Solar Energy Systems ISE in Freiburg and NREL, Germany, April 2017. Version 1.3.
- [3] S. Madala, R.F. Boehm, A review of nonimaging solar concentrators for stationary and passive tracking applications, *Renew. Sustain. Energy Rev.* 71 (2017) 309–322.
- [4] K. Shanks, S. Senthilarasu, T.K. Mallick, Optics for concentrating photovoltaics: trends, limits and opportunities for materials and design, *Renew. Sustain. Energy Rev.* 60 (2016) 394–407.
- [5] A.D. Vos, Detailed balance limit of the efficiency of tandem solar cells, *J. Phys. D Appl. Phys.* 13 (5) (1980) 839.
- [6] H. Hinterberger, R. Winston, Efficient light coupler for threshold Cerenkov counters, *Rev. Sci. Instrum.* 37 (1966a) 1094–1095.
- [7] S. Kurtz, D. Myers, W.E. McMahon, J. Geisz, M. Steiner, A comparison of theoretical efficiencies of multi-junction concentrator solar cells, *Prog. Photovoltaics Res. Appl.* 16 (6) (2008) 537–546.
- [8] F. Dimroth, Four-junction wafer bonded concentrator solar cells, *IEEE J. Photovolt.* 6 (2016) 343–349.
- [9] M. Adsten, B. Hellstrom, Measurement of radiation distribution on the absorber in an asymmetric CPC collector, *Sol. Energy* 76 (1–3) (2004) 199–206.
- [10] H. Hatwaambo, H. Hakansson, Angular characterization of low concentrating PV-CPC using low-cost reflectors, *Sol. Energy Mater. Sol. Cell.* 92 (11) (2008) 1347–1351.
- [11] D.I. Paul, M. Smyth, A. Zacharopoulos, J. Mondol, The design, fabrication and indoor experimental characterisation of an isolated cell photovoltaic module, *Sol. Energy* 88 (2013) 1–12.
- [12] W.T. Welford, R. Winston, *The Optics of Non-imaging Concentrators*, Academic Press, New York, NY, USA, 1978.
- [13] W.A.M. Al-Shohani, R.K. Al-Dadah, S. Mahmoud, A. Algareu, Optimum design of V-trough concentrator for photovoltaic applications, *Sol. Energy* 140 (2016) 241–254.
- [14] C.S. Sangani, C.S. Solanki, Experimental evaluation of V-trough (2 suns) PV concentrator system using commercial PV modules, *Sol. Energy Mater. Sol. Cells* 91 (2007) 453–459.
- [15] T.K. Mallick, P.C. Eames, T. Hyde, B. Norton, The design and experimental characterisation of an asymmetric compound parabolic photovoltaic concentrator for building facade integration in the UK, *Sol. Energy* 77 (3) (2004) 319–327.
- [16] T.K. Mallick, P.C. Eames, B. Norton, Power losses in an asymmetric compound parabolic photovoltaic concentrator, *Sol. Energy Mater. Sol. Cell.* 91 (12) (2007) 1137–1146.
- [17] A.K. Shukla, K. Sudhakar, P. Baredar, Recent advancement in BIPV product technologies: a review, *Energy Build.* 140 (2017) 188–195.
- [18] X. Wu, Y. Liu, J. Xu, W. Lei, J. Lin, Monitoring the performance of the building attached photovoltaic (BAPV) system in Shanghai, *Energy Build.* 88 (2015) 174–182.
- [19] N.M. Kumar, K. Sudhakar, M. Samyano, Performance comparison of BAPV and BIPV systems with c-Si, CIS and CdTe photovoltaic technologies under tropical weather conditions, *Case Stud. Therm. Eng.* 13 (2019), 100374.
- [20] B. Norton, P.C. Eames, T.K. Mallick, M.J. Huang, S.J. Mc Cormack, J.D. Mondol, Y.G. Yohanis, Enhancing the performance of building integrated photovoltaics, *Sol. Energy* 85 (8) (2011) 1629–1664.
- [21] A. Rabl, Comparison of solar concentrators, *Sol. Energy* 18 (2) (1973) 93–111.
- [22] A. Rabl, Optical and thermal properties of compound parabolic concentrators, *Sol. Energy* 18 (6) (1976) 497–511.
- [23] H. Hinterberger, R. Winston, Gas Cerenkov counter with optimized light-collecting efficiency, *Proc. Int. Instrum. High Energy Phys.* (1966b) 205–206.
- [24] V. Baranov, A paper in Russian that introduces certain properties of CPCs, *Opt. Mekh. Prom.* 6 (1965a) 1–5.
- [25] V. Baranov, G. Melnikov, Study of the illumination characteristics of hollow focons, *Sov. J. Opt. Technol.* (1966) 408–411.
- [26] V. Baranov, Eng transl: Parabolotoroidal mirrors as elements of solar energy concentrators, *Appl. Sol. Energy* 2 (1966) 9–12. *Geliotekhnika*, vol. 2, pp. 11–14.
- [27] R. Winston, Principles of solar concentrators of a novel design, *Sol. Energy* 16 (1974) 89–95.
- [28] M. Tiana, Y. Su, H. Zheng, G. Pei, G. Li, S. Riffat, A review on the recent research progress in the compound parabolic concentrator (CPC) for solar energy applications, *Renew. Sustain. Energy Rev.* 82 (Part 1) (2018) 1272–1296.
- [29] BISOL, *BISOL Datasheets*, Available: [http://www.bisol.com/images/Datasheets/EN/BISOL%20Product%20Specification%20BMO\\_EN.pdf](http://www.bisol.com/images/Datasheets/EN/BISOL%20Product%20Specification%20BMO_EN.pdf). (Accessed 12 February 2018).
- [30] Alanod, *MIRO-SILVER® Catalogue*, 2017. Available: [https://www.alanod.com/wp-content/uploads/2017/02/MIRO\\_SILVER\\_PD\\_8s\\_FINAL\\_D\\_E\\_11\\_14.pdf](https://www.alanod.com/wp-content/uploads/2017/02/MIRO_SILVER_PD_8s_FINAL_D_E_11_14.pdf). (Accessed 10 February 2018).
- [31] S. Ponce-Alcántara, J. Patrick Connolly, G. Sánchez, J. Manuel Míguez, V. Hoffmann, R. Ordás, A statistical analysis of the temperature coefficients of industrial silicon solar cells, in: 4th International Conference on Silicon Photovoltaics, *SiliconPV* 2014, vol. 55, 2014, pp. 578–588.
- [32] H. Singh, M. Sabry, D. Redpath, Experimental investigations into low concentrating line axis solar concentrators for CPV applications, *Sol. Energy* 136 (2016) 421–427.
- [33] D.A.G. Redpath, H. Singh, C. Tierney, P. Dalzell, An experimental comparison of two solar photovoltaic thermal (PVT) energy conversion systems for production of heat and power, *Energy Power* 2 (4) (2012) 46–50.